Local inversion symmetry breaking and spin-phonon coupling in the perovskite $GdCrO_3$

Sudipta Mahana,[1,2] Bipul Rakshit,[3] Raktima Basu,[4] Sandip Dhara,[4] Boby Joseph,[5] U. Manju,[6] Subhendra D. Mahanti,[7] and D. Topwal[1,2,*]

[1]*Institute of Physics, Sachivalaya Marg, Bhubaneswar 751005, India*
[2]*Homi Bhabha National Institute, Training School Complex, Anushakti Nagar, Mumbai 400085, India*
[3]*Center for Superfunctional Materials, Ulsan National Institute of Science and Technology, Ulsan 44919, South Korea*
[4]*Surface and Nanoscience Division, Indira Gandhi Centre for Atomic Research, HBNI, Kalpakkam 603102, India*
[5]*Elettra, Sincrotrone Trieste, Strada Statale 14, Km 163.5, Basovizza, 34149 Trieste, Italy*
[6]*CSIR-Institute of Minerals and Materials Technology, Bhubaneswar 751013, India*
[7]*Department of Physics and Astronomy, Michigan State University, East Lansing, Michigan 48824, USA*

(Received 20 June 2017; revised manuscript received 20 August 2017; published 12 September 2017)

Our detailed temperature-dependent synchrotron powder x-ray diffraction studies along with first-principles density-functional-theory-based calculations enable us to shed light on the origin of ferroelectricity in $GdCrO_3$. The actual lattice symmetry is found to be the noncentrosymmetric orthorhombic $Pna2_1$ structure, supporting the polar nature of the system. Polar distortion is associated with the Gd displacements with respect to the oxygen cage. Our study reveals an intimate analogy between $GdCrO_3$ and $YCrO_3$. However, a distinctive difference exists because Gd is less displacive than Y, which results in an orthorhombic $Pna2_1$ structure in $GdCrO_3$ in contrast to the monoclinic $P2_1$ structure in $YCrO_3$ and, consequently, decreases its polar property. It is found that magnetic coupling between Gd $4f$ and Cr $3d$ plays an important role in ferroelectric distortion. A strong magneto-electric coupling is also revealed using Raman spectroscopy based analysis, indicating its relevance to ferroelectric modulation.

DOI: 10.1103/PhysRevB.96.104106

I. INTRODUCTION

Multiferroics with the simultaneous existence of ferroelectricity and (anti)ferromagnetism have been of great interest over the past several decades not only for their potential technological applications but also for fundamental understanding. In spite of their huge potentials, multiferroic materials are rare because they have contradictory requirements, as magnetism requires an odd number of d electrons, while ferroelectricity generally occurs only in materials without d electrons [1]. This has led to an upsurge in research activities in this field aimed at identifying alternative mechanisms by which these degrees of freedom can coexist and couple strongly. Probably the best known ferroelectrics are ABO_3 perovskite-type oxides such as $BaTiO_3$ [2,3], in which ferroelectricity originates from the off-centering of Ti with respect to the oxygen octahedral cage due to the virtual hopping of electrons between empty Ti d and occupied O p states, whereas in $BiFeO_3$ [4] and $BiMnO_3$ [5] ferroelectricity is Bi $6s$ lone pair driven, which results in the displacement of the A-site ion from the centrosymmetric position with respect to the surrounding oxygen ions. Such ferroelectrics are classified as proper ferroelectrics, where the origin of ferroelectricity is a structural instability towards the polar state associated with electronic pairing [6].

In contrast, there exists a large variety of improper ferroelectrics such as orthorhombic rare-earth manganites ($RMnO_3$, R = Gd, Tb, Dy) [6–8] in which ferroelectricity arises due to the breaking of inversion symmetry from the spiral spin order. The underlying mechanism for the generation of electric polarization is the inverse Dzyaloshinskii-Moriya interaction, where the spin configuration displaces oxygen (ligand) ions through the electron-lattice interaction or through a spin-current model [9]. Another mechanism that can lead to ferroelectricity is charge ordering, in which B sites contain transition-metal ions with different valency, for example, $RNiO_3$ [10]. In hexagonal rare-earth manganites ($RMnO_3$, R = Ho-Lu, Y) polarization arises from the tilting of MnO_5 polyhedra accompanied by displacement of the R ions; therefore they have been coined improper geometric ferroelectrics [6,11]. Apart from these a low-temperature ferroelectric phase has been observed in Gd(Dy)FeO_3, which arises due to the exchange striction between Gd(Dy) and Fe spins [12,13]. Perovskite $CdTiO_3$ is a unique system, in which ferroelectricity is driven by a phase transition from the centrosymmetric orthorhombic structure ($Pbnm$) to a noncentrosymmetric structure ($Pna2_1$) via displacement of Ti and O ions, even though overall orthorhombic symmetry is maintained [14,15]. Recently, a new mechanism was proposed in which the rotation of oxygen octahedra coupled with lattice distortion leads to a ferroelectric phase [16–18].

Moreover, there are diverging opinions about the existence and/or origin of ferroelectricity in rare-earth orthochromites ($RCrO_3$). Most of the members of the $RCrO_3$ family have been predicted to be biferroic with a reasonably high ferroelectric (FE) transition temperature (above the magnetic transition temperature), caused by polar movement of R ions associated with phonon instability at the zone center as in other perovskite ferroelectrics like $PbTiO_3$ [19–22]. From neutron pair distribution function (PDF) analysis, $YCrO_3$ has been reported to possess a locally noncentrosymmetric monoclinic structure ($P2_1$) via Cr off centering in the ferroelectric state although the average crystal structure is centrosymmetric ($Pnma/Pbnm$) [23]. The structural instability was also supported from theoretical calculations; however, this polar instability mode is associated with Y displacements in a direction opposite

*dinesh.topwal@iopb.res.in, dinesh.topwal@gmail.com

that of the oxygen cage and Cr atom [19,20]. It suggests that local noncentrosymmetry could play an important role in understanding the ferroelectric properties in the family of $R\mathrm{CrO_3}$ [24].

In addition to the structural distortion ideas in which the magnetic coupling plays a minor role, several studies have reported that the multiferroicity in $R\mathrm{CrO_3}$ is due to the strong interaction between magnetic R and weakly coupled ferromagnetic (canted) Cr ions below the magnetic ordering temperature of Cr T_N along with a symmetry structure lower than $Pbnm$ [24,25]. Also, Raman studies show an anomalous change in phonon frequency and a decrease in phonon lifetimes across the multiferroic transition temperature, both in the modes involving $\mathrm{CrO_6}$ octahedra and the magnetic R ion [26]. This argument implies that ferroelectricity in $R\mathrm{CrO_3}$ is driven by a magnetostriction mechanism caused by $3d$-$4f$ coupling, resulting in the displacement of the R ion and the octahedral distortion via oxygen displacements. This suggests that one has to have a magnetic R ion in order to stabilize a ferroelectric state in $R\mathrm{CrO_3}$. Recently, some $R\mathrm{CrO_3}$ (R = Sm and Ho) compounds underwent structural transformation from centrosymmetric $Pbnm$ to the noncentrosymmetric $Pna2_1$ subgroup, which is responsible for the polar order [27,28]. In these systems magnetic coupling between the R ion and the matrix is not important in stabilizing a ferroelectric phase as it develops in the paramagnetic state. On the contrary, recently, it was reported that $\mathrm{GdCrO_3}$ can be ferroelectric only at very low temperature via the magnetostriction effect, and it is necessary to have $\mathrm{Gd^{3+}}$-$\mathrm{Cr^{3+}}$ interaction and a G-type magnetic structure in both Gd and Cr sublattices to break the inversion symmetry as driven by antipolar X-mode instability [29]. Considering all the contradicting possibilities, it is important to understand the microscopic origin and mechanism of ferroelectricity in $\mathrm{GdCrO_3}$ at relatively high temperatures.

In this paper we discuss the results of detailed studies on the possible noncentrosymmetric structure of $\mathrm{GdCrO_3}$ using x-ray diffraction (XRD) measurements and first-principles calculations. We also investigate the possible polar phonon mode instability in its cubic structure as it plays a crucial role in understanding classic ferroelectrics. Further, we also discuss the magnetoelectric coupling in the material from temperature-dependent Raman measurements.

II. EXPERIMENTAL AND THEORETICAL METHODS

The $\mathrm{GdCrO_3}$ sample was prepared using the solid-state reaction method as reported elsewhere [30,31]. Phase purity of the sample was confirmed by powder XRD measurements carried out in a D8 advanced diffractometer equipped with Cu $K\alpha$ radiation while the magnetic and physical properties were confirmed by physical property measurement system (PPMS). Temperature-dependent XRD measurements were performed at the XRD1 beamline at the Elettra synchrotron radiation facility using photons with a wavelength of 0.85507 Å. Rietveld refinements of the diffraction patterns were performed using the FULLPROF package. The vibrational properties of the sample were measured using a micro-Raman spectrometer (inVia, Renishaw, United Kingdom) with 514.5-nm excitation of an $\mathrm{Ar^+}$ laser. Spectra were collected in the backscattering configuration using a thermoelectrically cooled CCD camera as the detector. A long working distance 50× objective with a numerical aperture of 0.45 was used for the spectral acquisition. In order to carry out the temperature-dependent Raman spectroscopic measurements, the sample was kept in a Linkam (THMS600) stage, driven by an autocontrolled thermoelectric heating and cooling function within a temperature range of 80 to 300 K.

Our theoretical calculations of the structural properties were based on density-functional theory, using the generalized gradient approximation with the Perdew-Burke-Ernzerhof for solids (PBEsol) [32] parametrization for the exchange-correlation potential, the projector augmented-wave (PAW) method [33], and a plane-wave basis set, as implemented in the Vienna Ab initio Simulation Package (VASP) [34]. The interaction between ions and electrons was approximated with PAW potentials, treating $3p$, $3d$, and $4s$ for Cr and $2s$ and $2p$ for O as valence electrons. For Gd, the $4f$ state was treated as either a valence state or as a core state. Hubbard U was used for better treatment of Cr $3d$ and Gd $4f$ electrons and was chosen to be 3 and 4 eV for Cr and Gd, respectively, in line with an earlier report [29]. For Brillouin zone sampling, we chose 12×12×8 and 6×6×6 Monkhorst-Pack k-point meshes [35] for orthorhombic and cubic structures, respectively, and the wave function was expanded in a basis set consisting of plane waves with kinetic energies less than or equal to 770 eV. Using these parameters, an energy convergence of less than 1 meV/f.u. was achieved. Structures were fully relaxed until residual Hellmann-Feynman (HF) forces were smaller than 0.001 eV/Å while maintaining the symmetry constraints of the given space group. The G-type magnetic structure was considered for both Cr and Gd moments in the calculation [29,36]. In order to impose G-type antiferromagnetic ordering in a cubic structure, the unit cell was doubled along the ⟨111⟩ direction, which resulted in a ten-atom unit cell [20]. The phonon frequencies were calculated in high-symmetry directions using the 2×2×2 supercell. The real-space force constants of the supercell were calculated using density-functional perturbation theory (DFPT) implemented in the VASP package. The unit cell results in 30 phonon branches: 3 acoustic which have a zero frequency at k = (0,0,0) and 27 optical, some of which are triply degenerate. We are mainly interested in optical modes with imaginary phonon frequencies corresponding to instabilities in the structure. Due to the doubling of the unit cell along the ⟨111⟩ direction, we could access zone-boundary phonon modes at the R point along with the zone-center Γ modes [20]. The electric polarization was calculated using the Berry phase method [37], as implemented in VASP. The utility tool PHONOPY [38] was used to obtain phonon frequencies and phonon dispersions over the entire Brillouin zone.

III. RESULTS AND DISCUSSION

$\mathrm{GdCrO_3}$ crystallizes in perovskite structure with Goldschimdt's tolerance factor, $t = \frac{(r_{Gd^{3+}} + r_{O^{2-}})}{\sqrt{2}(r_{Cr^{3+}} + r_{O^{2-}})} = 0.862$, indicating an orthorhombically distorted structure [39,40]. Figures 1(a) and 1(b) depict synchrotron x-ray diffraction patterns acquired at 300 and 100 K, respectively, along with the corresponding

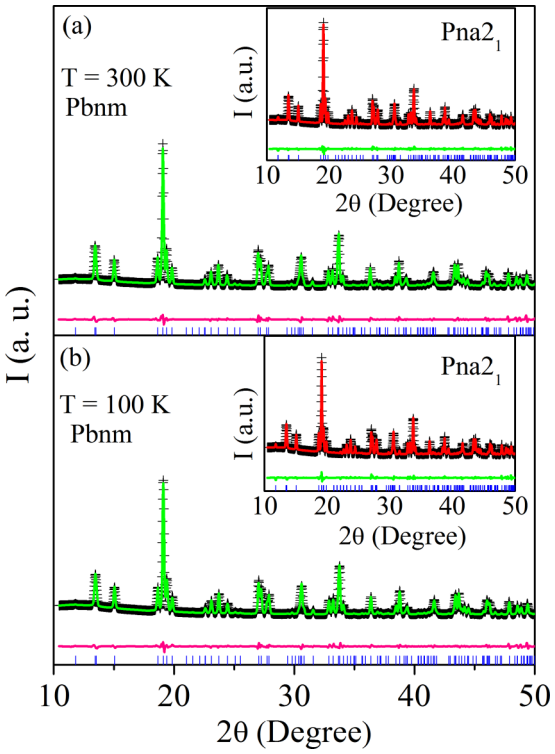

FIG. 1. X-ray powder diffraction patterns (symbols) obtained at (a) 300 K and (b) 100 K with the refinement patterns (solid curve) using the $Pbnm$ space group superimposed on it. Insets represent the same with Rietveld refinement using the $Pna2_1$ space group.

Rietveld refined data using the $Pbnm$ space group superimposed on it. Reasonably small values of reliability parameters (for 300 K, $R_w \sim 0.084, R_{\rm exp} \sim 0.041$, and $\chi^2 \sim 4.16$, while for 100 K, $R_w \sim 0.088, R_{\rm exp} \sim 0.043$, and $\chi^2 \sim 4.23$) indicate the good quality of the fitting and suggest that the centrosymmetric $Pbnm$ space group persists in the entire (studied) temperature range. Additionally, the compound undergoes a G-type magnetic ordering in the Cr sublattice below $T_N = 169$ K [24,36] (whereas the Gd sublattice remains in the paramagnetic state). A weak electric polarization is also observed at the same temperature, suggesting the polar nature of the system [24]. It has to be noted that globally centrosymmetric magnetic and crystal structures are not compatible with the observation of ferroelectric phase. This strongly indicates the possibility of a local noncentrosymmetric structure in $GdCrO_3$, which might be responsible for its ferroelectric property.

Recent synchrotron x-ray diffraction studies on the other members of the rare-earth chromite family ($RCrO_3$, R = Sm, Ho, and Nd) over a wide temperature range reveal a structural transition from the high-temperature centrosymmetric $Pbnm$ space group to the low-temperature noncentrosymmetric $Pna2_1$ subgroup close to the onset of polar order [27,28,41]. Also, it has been proposed that local noncentrosymmetry drives ferroelectricity in $YCrO_3$, although its average crystal structure is centrosymmetric [19,23]. Keeping this in mind, XRD patterns of $GdCrO_3$ were also refined with the noncentrosymmetric $Pna2_1$ space group as depicted in the insets of Fig. 1, and the reliability parameters are surprisingly similar to the $Pbnm$ space group for both 300 and 100 K ($R_w \sim 0.083, R_{\rm exp} \sim 0.041$, and $\chi^2 \sim 4.37$ for 300 K and $R_w \sim 0.082$, $R_{\rm exp} \sim 0.041$, and $\chi^2 \sim 3.94$ for 100 K), suggesting that the average long-range ordering as depicted by x-ray diffraction cannot provide an answer to the origin of ferroelectricity in $GdCrO_3$ on its own.

We hence performed first-principles density-functional calculations with fully optimized structure using the PBEsol functional [32], as it was shown to be quite accurate in the estimation of lattice parameters and to describe the ferroelectric property best [42,43]. We fully optimized the structure of $GdCrO_3$ using the $Pbnm$ space group and found that the resulting structure attains noncentrosymmetric $Pna2_1$ symmetry, which was confirmed using FINDSYM software [44,45]. In order to further confirm the results, we did calculations considering the $Pbnm$ and $Pna2_1$ structures separately and observed that both the structures converge to structures having the same lattice parameters. The optimized lattice parameters for the $Pna2_1$ structure are $a = 5.530$ Å, $b = 5.306$ Å, and $c = 7.601$ Å. The energy difference is less than 1 meV (0.3 meV/f.u.), which is within calculation error. We believe that the ground-state structure of $GdCrO_3$ is noncentrosymmetric $Pna2_1$, as it favors nonzero polarization. However, the distortion in the structure might be very small; hence, it is not distinguished by XRD measurements. Recent theoretical calculations allowing for magnetic interaction for different crystal symmetries by Zhao *et al.* suggested that only $Pna2_1$ crystal symmetry gives a sizable polarization for $GdCrO_3$, which is in agreement with our results [29]. However, according to them, $GdCrO_3$ can be ferroelectric only at very low temperature as it is necessary to have magnetic ordering in the Gd sublattice (G type) along with that of the Cr sublattice to break the inversion symmetry *via* the exchange-striction mechanism, which is associated with antipolar X-mode instability in the ideal cubic perovskite. We observed noncentrosymmetric $Pna2_1$ symmetry in $GdCrO_3$ both when Gd $4f$ electrons were treated as valance electrons and when they were treated as core electrons. This suggests that magnetic coupling between Cr and Gd moments is not necessary for the stability of the $Pna2_1$ structure. However, the actual positions of the atoms and the value of the ferroelectric moment do depend on whether Gd $4f$ electrons are treated as core or valence states.

To understand the origin of ferroelectricity in $GdCrO_3$ at relatively high temperature we performed phonon calculations using the density-functional perturbation theory approach for the ideal cubic perovskite structure of $GdCrO_3$ to access various structural instabilities in the system. Structural instability studies have been used to examine a large variety of ferroelectric perovskite oxides [19–22,46,47]. As the structure was fully relaxed using the PBEsol functional, the resulting lattice constant was found to be only 0.3% (0.5%) less than that of the experimental value considering Gd $4f$ electrons as the valence (core) state. Calculated phonon dispersion curves treating Gd $4f$ as the core state are shown in Fig. 2, with imaginary frequencies plotted in the negative axis. Soft modes occur over a wide range of wave vectors, with strong instabilities at the R (R_{25}) and M (M_3) symmetry points which are associated with the octahedral rotations. Simultaneous condensation of these soft modes results in cubic-to-orthorhombic phase transition.

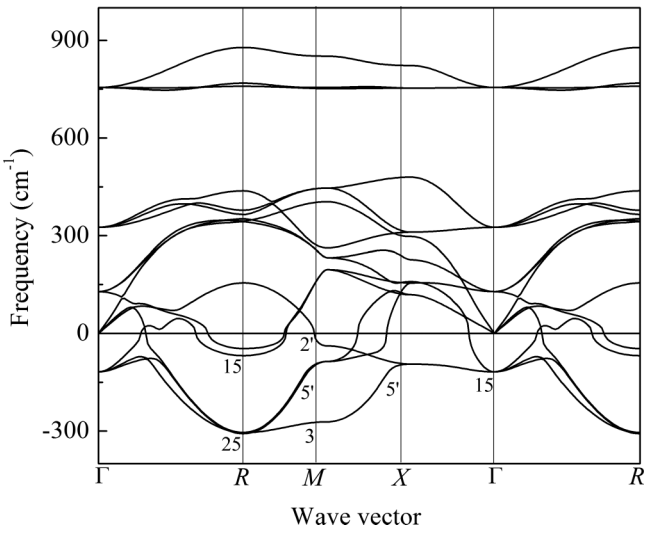

FIG. 2. Phonon dispersion curves for the cubic phase of $GdCrO_3$ treating Gd $4f$ as a core state. The labels indicate the symmetry of unstable modes.

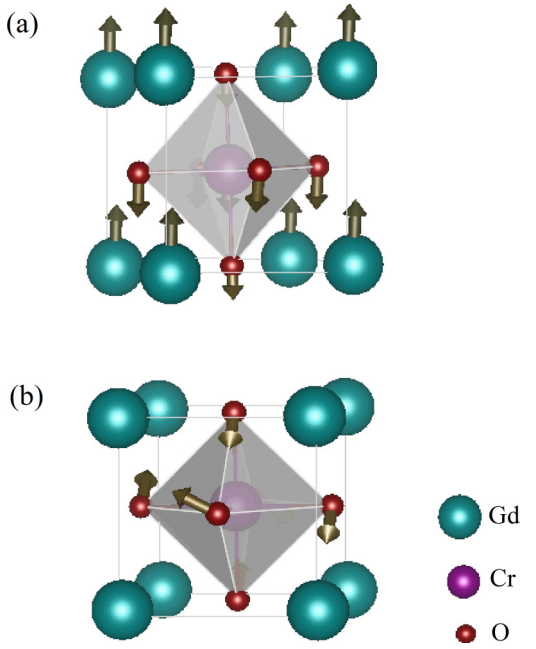

FIG. 3. Visualization of eigenvectors of unstable (a) polar Γ_{15} and (b) antiferrodistortive R_{25} modes.

Polar mode instabilities at the R, X, and Γ points are associated with displacements of Gd and oxygen atoms, a case similar to that for $YCrO_3$ [19]. Modes at the R (R_{15}) and X ($X_{5'}$) points correspond to antiferroelectric distortions and can give rise to only nonzero polarization below the Gd ordering temperature via the magnetostriction effect with the dominant contribution from the X mode, as reported by Zhao *et al.* [29]. The Γ (Γ_{15}) mode, on the other hand, is responsible for the polarization at relatively high temperature, as described in $YCrO_3$ and other ferroelectric perovskite compounds [19,20,22].

To understand more, we also determined phonon frequencies at the Γ point, which gave phonons at the Γ and R points of the primitive unit cell due to the doubling of the unit cell along the $\langle 111 \rangle$ direction. Treating Gd $4f$ as the core state, we found one triply degenerate zone-center instability at $120i$ cm^{-1} (Γ_{15}) and two triply degenerate zone-boundary instabilities at $60i$ cm^{-1} (R_{15}) and $302i$ cm^{-1} (R_{25}), similar to $YCrO_3$ and other d^3 systems [20]. Considering Gd $4f$ as the valence state in the calculations, we noticed R_{15} is no longer unstable, while the magnitudes of the other two modes decrease as $293i$ cm^{-1} (R_{25}) and $92i$ cm^{-1} (Γ_{15}). This clearly indicates a strong influence of Gd $4f$ electrons on the various instability modes of the cubic structure.

The weakest instability mode, R_{15}, involves the displacement of the Gd cations along with small oxygen displacements, and these are antiparallel in neighboring unit cells. The Γ_{15} mode [Fig. 3(a)] involves mainly the Gd ion movement in a direction opposite that of the oxygen cage and Cr ions, whereas Cr and O ions move in the same direction, resulting in a ferroelectric polar structural distortion very similar to that of $YCrO_3$ [19,20]. The strongest instability, R_{25} [Fig. 3(b)], is an antiferrodistortive (AFD) mode corresponding to the rotation of the corner-connected oxygen octahedra. To probe the strength of ferroelectric instability, we displaced the atoms toward the eigenvectors for the polar Γ_{15} mode and relaxed it, which resulted in an energy lowering by 0.90 eV/f.u.

We calculated the magnitude of ferroelectric polarization using the Berry phase method and found it to be 0.75 μC/cm^2 when the Gd $4f$ electrons were treated as valence electrons. The strength of the polarization decreased to 0.35 μC/cm^2 when the $4f$ electrons were treated as the core state. This indicates that magnetic exchange coupling between Gd $4f$ and Cr $3d$ electrons does play an important role in ferroelectric distortion. The value of 0.75 μC/cm^2 is in close agreement with the experimental value ($\sim$0.7 μC/cm^2) [24]. The XX component of calculated Born effective charges (BECs) are listed in Table I. The BEC tensor $Z^*_{i,\alpha\beta}$ is described as the change in the polarization component P_α resulting from a displacement ∂r of ion i along Cartesian direction β [48,49],

$$Z^*_{i,\alpha\beta} = \frac{\Omega}{|e|}\frac{\partial P_\alpha}{\partial r_{i,\beta}}, \tag{1}$$

where Ω is the unit-cell volume and e is the electronic charge. A significantly enhanced BEC of Gd compared to its formal charge indicates large changes in hybridization of Gd with the surrounding ions, which is a smoking gun for the emergence of ferroelectricity. It is surprising that the polarization value in $GdCrO_3$ is one order of magnitude less than that of $YCrO_3$ [19], even though the BEC of Gd is comparable to that of Y, as given in Table I. Also note that BECs are not affected by whether one considers Gd $4f$ a valance state or inside the core. However, BEC alone cannot define the tendency of a

TABLE I. The XX component of the Born effective charge tensor for cubic $GdCrO_3$ compared with $YCrO_3$ [20]. Formal charges are given in parentheses.

Compound	$Z^\star_{Gd/Y}$	$Z^\star_{Cr}$	$Z^\star_{O_x}$	$Z^\star_{O_{y,z}}$
$GdCrO_3$ (with Gd $4f$)	4.55(3)	3.33(3)	−3.49(−2)	−2.16(−2)
$GdCrO_3$ (without Gd $4f$)	4.48(3)	3.32(3)	−3.48(−2)	−2.16(−2)
$YCrO_3$	4.45(3)	3.44(3)	−2.62(−2)	−2.66(−2)

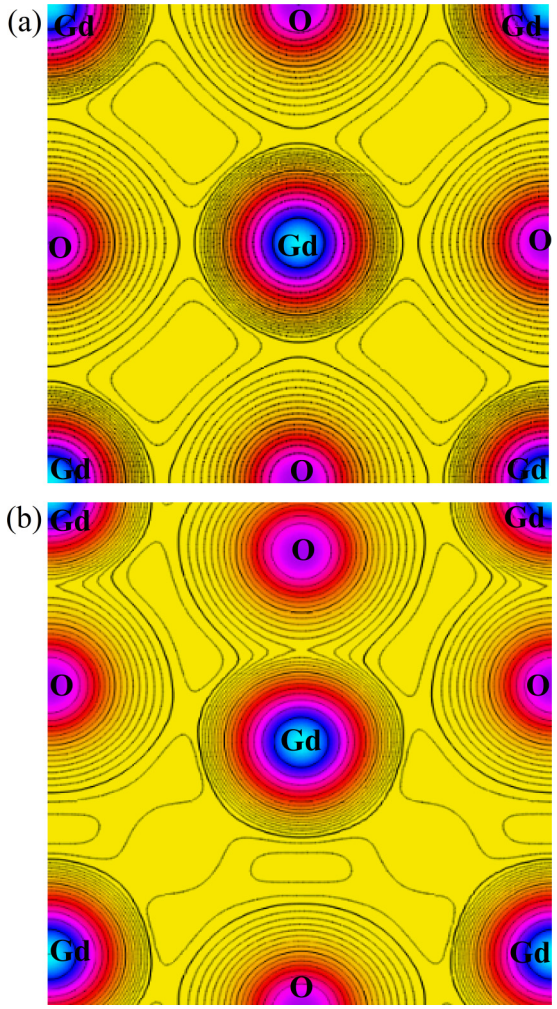

FIG. 4. Contour plots of charge density around the O-Gd-O bonds in the [001] plane of (a) undistorted cubic $GdCrO_3$ and (b) distorted $GdCrO_3$ associated with the frozen-in ferroelectric phonon mode Γ_{15}.

certain material towards ferroelectricity [49]. Also the ionic radii of Gd^{3+} (1.08 Å) and Y^{3+} (1.04 Å) ions are similar, indicating that the reduction in the strength of polarization in the Gd system is not due to the effect of the size of the R site like in $LaCrO_3$. The difference in their polarizations arises from the smaller displacement of Gd compared to Y and is possibly due to the subtle forces involving Gd orbitals (filled or unfilled) either directly or indirectly. Additionally, the BEC for Cr here is similar to the value found for $YCrO_3$ and other $RCrO_3$ (R = Lu and La) [20]. An anomalous BEC is obtained for O_x which is similar to the value found in $LaCrO_3$ with a very high magnetic transition temperature and quite large compared to the value for $YCrO_3$ with a low magnetic transition temperature [20,21]. This suggests that the larger BEC in O_x is due to the stronger Cr-O-Cr superexchange interaction, consequently, having a relatively higher magnetic transition temperature in $GdCrO_3$ than $YCrO_3$.

The charge densities around the O-Gd-O bonds in the [001] plane of the undistorted cubic structure and the distorted structure associated with the frozen-in ferroelectric phonon mode Γ_{15} are shown in Figs. 4(a) and 4(b), respectively. The charge density around the Gd ion for the undistorted cubic structure is quite spherical, and the Gd-O hybridization is minimal. The ferroelectric distortion causes the Gd and O ions to displace in opposite directions [Fig. 3(a)], which results in one pair of Gd and O ions closer together and builds up large charge density in the Gd-O bond, indicating an increase in Gd-O hybridization, as shown in Fig. 4(b). This indicates ferroelectric instability results in asymmetric stretching of the O-Gd-O bond and suggests that Gd-site partial covalency is the driving force for the ferroelectric distortion in the compound.

Further, to see the effect of intrasite Coulomb correlation effects of Cr $3d$ and Gd $4f$ electrons on the structural properties and on phonon modes we also did calculations without U and found the same negative modes ($\Gamma_{15} \sim 67i$ cm^{-1} and $R_{25} \sim 266i$ cm^{-1}); however, both the modes are affected noticeably. Correlations lead to softening of both modes by about 25 cm $^{-1}$.

Ferroelectric behavior in $GdCrO_3$ is based on the competition between the polar (Γ_{15}) mode and the AFD rotational (R_{25}) mode [50,51]. The polar mode favors the noncentrosymmetric ferroelectric phase, whereas the AFD mode (octahedral rotation) hinders the ferroelectric ordering by inducing R-site antipolar displacements and results in centrosymmetric phase. The competition between these two modes stabilize various structures as follows. The ferroelectric rhombohedral structure is associated with only polar instability without having AFD instability. However, a progressive increase of AFD instability combined with the decrease of polar instability gives rise to monoclinic, tetragonal, and orthorhombic phases, respectively, which in turn suppress the ferroelectric property in the structure gradually [50]. It can be noted that both polar and AFD modes are weaker in $GdCrO_3$ than in $YCrO_3$ [20]. The dominant contribution of the AFD mode together with the ferroelectric mode results in the $Pna2_1$ phase in $GdCrO_3$ and reduces the ferroelectric property compared to $YCrO_3$, which stabilizes in the monoclinic $P2_1$ phase [23]. The intrinsic differences in the bonding in monoclinic $YCrO_3$ and orthorhombic $GdCrO_3$ leads to different magnitudes of polarization.

As discussed previously, XRD and theoretical studies reveal the probable noncentrosymmetric $Pna2_1$ crystal structure in the ferroelectric state for $GdCrO_3$. Displacements of Gd atoms combined with AFD distortion of octahedra via movements of specific oxygen ions lift certain symmetries of the centrosymmetric $Pbnm$ structure and stabilize the lower-symmetry $Pna2_1$ structure. In short, there is a coupling and competition between AFD zone-boundary and polar zone-center instabilities, and consequent structural rearrangements are responsible for the emergence of spontaneous polarization.

In addition to the structural studies through x-ray diffraction, we also performed temperature-dependent Raman spectroscopy studies. This is a powerful and sensitive technique for detecting subtler structural rearrangements and microscopic changes across the phase transitions such as the evolution of phonons, magnons, and electromagnons in multiferroic materials. Based on group-theoretic analysis of the orthorhombic structure 24 first-order Raman active modes are expected for $GdCrO_3$ which are classified as $\Gamma_{\text{Raman}} = 7A_g + 5B_{1g} + 7B_{2g} + 5B_{3g}$, involving vibration of Gd and oxygen atoms [52]. Figure 5 depicts the temperature-dependent Raman spectra at a few select temperatures both below and above

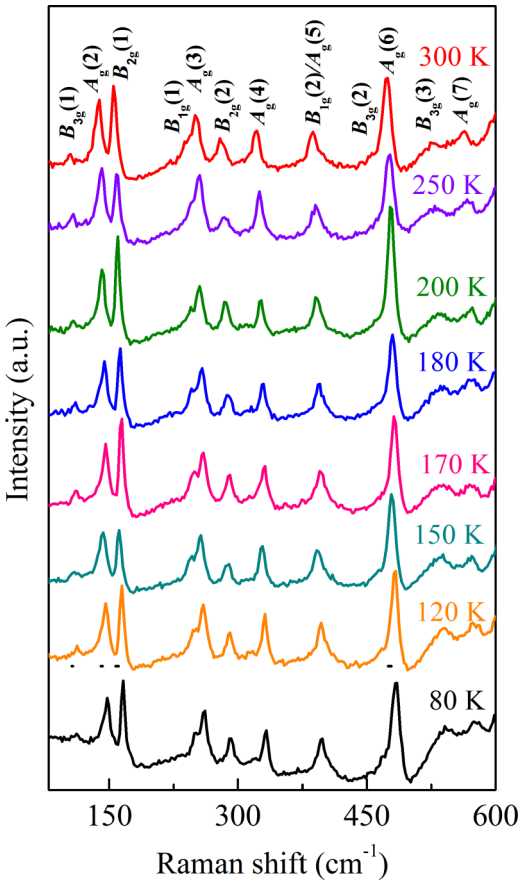

FIG. 5. Raman spectra of $GdCrO_3$ at a few selective temperatures both above and below the magnetic/ferroelectric ordering temperature (169 K).

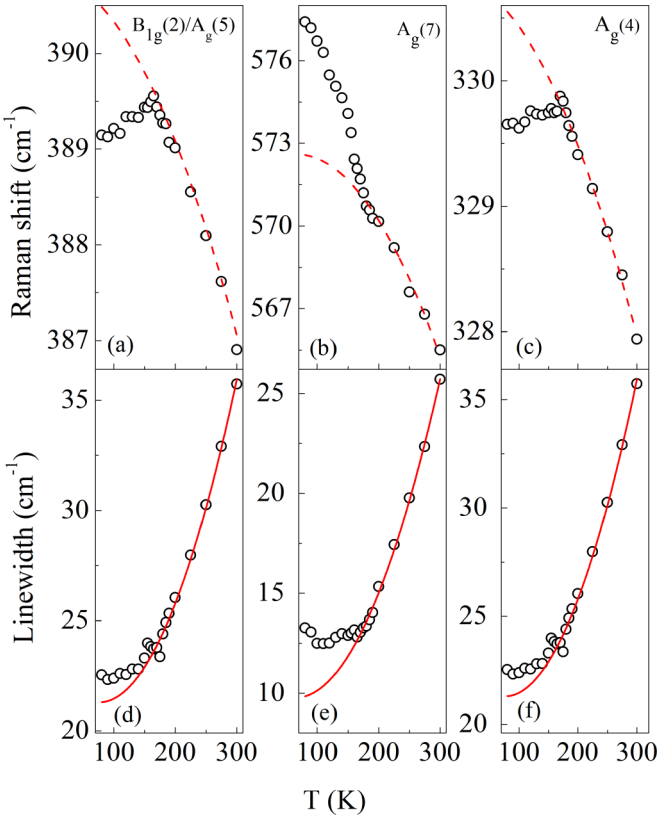

FIG. 6. (a)–(c) Temperature dependence of frequencies of a few selective modes: octahedral rotation with respect to the y axis $[B_{1g}(2)/(A_g(5)]$, antisymmetric stretching $[A_g(7)]$, and Gd-O vibration $[A_g(4)]$, respectively. The dashed lines represent the fitted curves for anharmonic contributions to these modes according to Eq. (2). (d)–(e) Linewidths of the corresponding modes; solid lines represent the fitted curves for anharmonic contributions according to Eq. (2).

the transition temperature. We see only 14 Raman modes. The absence of other predicted modes is due to very low intensity, which is below the detection limit of the instrument or beyond our experimental range. The phonon modes below 200 cm^{-1} generally arise from the movement of Gd atoms. $B_{1g}(1)$ and $A_g(3)$ involve out-of-phase and in-phase octahedral z rotations, respectively. $B_{2g}(2)$ and $A_g(4)$ are related to Gd-O vibrations in GdO_{12} polyhedra. $B_{1g}(2)/A_g(5)$ involve the out-of-phase/in-phase octahedral y rotations, and $B_{3g}(2)$ is associated with out-of-phase bending. $A_g(6)$ involves the octahedral bending mode, $B_{3g}(3)$ is associated with in-phase O_2 scissorlike vibration, and $A_g(7)$ arises from antisymmetric stretching vibration of octahedra [26,52–54].

At first glance, no new modes emerge down to 80 K from 300 K. Further, to examine the subtle structural changes and the presence of any interactions between lattice and magnetic degrees of freedom, i.e., spin-phonon coupling, the Raman spectra were analyzed by Lorentzian fitting of the peaks. The intrinsic anharmonic contribution to the temperature variation of the phonon frequency of various Raman modes can be explained by the following relation [55]:

$$\omega_{anh}(T) = \omega(0) - A\left[1 + \frac{2}{e^{\frac{\hbar\omega(0)}{2k_BT}} - 1}\right] - B\left[1 + \frac{3}{e^{\frac{\hbar\omega(0)}{3k_BT}} - 1} + \frac{3}{(e^{\frac{\hbar\omega(0)}{3k_BT}} - 1)^2}\right], \quad (2)$$

where $\omega(0)$ is the frequency at $T = 0$ K of the mode in the harmonic approximation, T is in kelvins, and A and B are anharmonicity coefficients for cubic and quartic anharmonic processes, respectively.

Figure 6(a) represents the temperature evolution mode associated with the out-of-phase/in-phase octahedral y rotations $[B_{1g}(2)/A_g(5)$; represented as circles], along with their fitting using Eq. (2) (marked by the dashed line). Below the transition, it shows a pronounced softening from the intrinsic anharmonic contribution. The anomalous behavior of this phonon mode across T_N can be explained by the exchange-striction effect. To understand more about the origin of the anomalous behavior of various phonon modes such as the presence of spin-phonon coupling, it is necessary to study the temperature dependence of corresponding linewidths as these are related to the phonon lifetime, which will not be affected by subtle volume changes due to the exchange-striction effect.

Figure 6(d) shows the temperature evolution of the linewidth of the mode related to octahedral rotations. The anomaly in the linewidth across the transition indicates the presence of spin-phonon coupling in $GdCrO_3$. Such spin-phonon coupling was not observed in $RCrO_3$ with nonmagnetic R^{3+} ions such as Y, Lu, etc. [26]. This suggests the presence of

spin-phonon coupling due to the magnetic interaction between Gd^{3+} and Cr^{3+} moments, which is mediated by the weak ferromagnetic coupling (canted) of the Cr sublattice. The temperature variations of the frequency and the corresponding linewidth of the antisymmetric stretching mode [$A_g(7)$] are shown in Figs. 6(b) and 6(e), respectively. Such hardening behavior of the antisymmetric stretching mode in $YCrO_3$ has been explained by the exchange-striction effect with a major contribution of 30%−40% and the remaining contribution coming from magnetic coupling (Cr^{3+}-Cr^{3+} interaction) [52]. Thus spin-phonon coupling cannot be ignored in $YCrO_3$, although no significant anomaly in linewidth was seen by Bhadram *et al.* in this system [26]. Similarly, in $GdCrO_3$ the hardening behavior of the antisymmetric stretching mode can be explained by the exchange-striction effect, consistent with the reduction of the unit-cell volume. In addition, a pronounced anomaly is observed in the linewidth. This indicates a strong spin-phonon coupling, which can be explained by the Gd^{3+}-Cr^{3+} interaction in addition to a contribution from the Cr^{3+}-Cr^{3+} interaction. Sharma *et al.* also observed considerable softening of the bending mode along with the anomaly in its linewidth in $YCrO_3$ (nonmagnetic *R* ion) [56], favoring a significant contribution of the Cr^{3+}-Cr^{3+} magnetic interaction to the spin-phonon coupling below the magnetic transition as discussed here. Moreover, lattice modes related to Gd atoms also show strong softening below the transition along with anomalies in their linewidths, as clearly seen in the $A_g(4)$ mode [Figs. 6(c) and 6(f)]. This suggests a possible displacement of the Gd^{3+} ion induced by the spin-phonon coupling caused by Gd^{3+}-Cr^{3+} interaction [26].

As discussed above, the anomalous behavior of various modes is mainly due to the exchange-striction effect (lattice contribution) and spin-phonon coupling induced by Cr^{3+}-Cr^{3+} and Gd^{3+}-Cr^{3+} interactions right below the magnetic transition. Granado *et al.* proposed that the spin-phonon coupling strength can be estimated for a given mode by relating the deviation of the Raman mode frequency from the intrinsic anharmonic contribution to the nearest-neighbor spin-spin correlation function ($\mathbf{S}_i \cdot \mathbf{S}_j$) as given by [57]

$$\Delta\omega_{sp-ph} = \lambda\langle \mathbf{S}_i \cdot \mathbf{S}_j \rangle, \tag{3}$$

where λ is the spin-phonon coupling coefficient. In the molecular field approximation, the spin-spin correlation function can be described by the square of the sublattice magnetization [58] and also by the normalized order parameter [59]. The temperature dependence of the frequency mode can be written as follows:

$$\Delta\omega_{sp-ph} = \lambda S^2\left[1 - \left(\frac{T}{T_N}\right)^{\gamma}\right] \approx \lambda\left(\frac{M(T)}{M_{\max}}\right)^2, \tag{4}$$

where T_N is the Cr ordering temperature, $S = 3/2$ is the spin quantum number of the Cr^{3+} ion, γ is the critical exponent, and $M(T)$ is the magnetization as a function of temperature T.

Since different modes involve motions of different atoms, the associated coupling constant λ depends on how these motions change the bond lengths and bond angles involving the oxygen atoms which mediate magnetic exchange. As the antisymmetric stretching mode [$A_g(7)$] exhibits the largest deviation from the conventional anharmonic behavior below the transition, it should correspond to possibly the largest value of spin-phonon coupling. Figure 7 shows the thermal evolution of $\Delta\omega_{sp-ph}$ below T_N (circles) and its fitting with Eq. (4) (dashed line). The good fit obtained by considering only the symmetric Cr^{3+}-Cr^{3+} interaction implies that the antisymmetric interaction (canted ferromagnetism) is very weak. We also found symmetric exchange coupling ($J_e = 11.06$ K) is four times larger than the antisymmetric Dzyaloshinskii-Moriya interaction ($D = 2.64$ K) by fitting the temperature dependence of magnetization with a modified Curie-Weiss law given by Moriya [31,60,61]. From the fitting, a spin-phonon coupling constant λ of 3.02 cm^{-1} and critical exponent γ of 2.9 are obtained, while the value of λ calculated from sublattice magnetization yields a spin-phonon coupling constant λ of 2.8 cm^{-1}, which is in good agreement with that estimated from the order parameter. The obtained spin-phonon coupling in $GdCrO_3$ is quite comparable to the various systems estimated from Raman modes. For example, in antiferromagnetic rutile-structured MnF_2 and FeF_2 [62] the spin-phonon coupling strengths for different modes are in the range from 0.4 to 1.3 cm^{-1}, and for $Sr_4Ru_3O_{10}$ [63], λ is 5.2 cm^{-1}. The above estimated coupling constant considers only the nearest-neighbor Cr^{3+}-Cr^{3+}. In addition, there is an important contribution from the Gd^{3+}-Cr^{3+} interaction to spin-phonon coupling, as discussed above. These results corroborate the existence of strong magnetoelectric coupling in the system, as evidenced by the dielectric measurement and the enhancement of polarization with magnetic field [24,26].

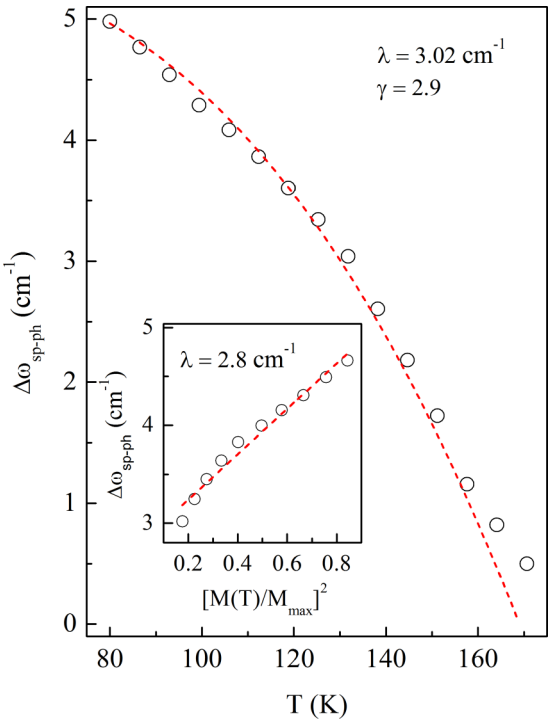

FIG. 7. Temperature dependence of $\Delta\omega$ of the stretching mode [$A_g(7)$] below T_N. The dashed line represents the fitting using Eq. (4). The inset shows $\Delta\omega$ versus $[M(T)/M_{\max}]^2$ (circles) and its fitting (dashed line) using Eq. (4).

IV. CONCLUSION

In conclusion, our results clearly demonstrate that the preferred symmetry of $GdCrO_3$ is noncentrosymmetric $Pna2_1$. Our calculations also support the observed ferroelectricity in $GdCrO_3$ through the determination of the detailed structure. There are competing structural instabilities in $GdCrO_3$, and the dominating one is of antiferrodistortive type; the weak polarization arises from the small ferroelectric instability resulting in Gd-O bond polarization. The smaller displacement of Gd than that of Y leads to a decrease in the strength of ferroelectricity in $GdCrO_3$ compared to $YCrO_3$, indicating a strong influence of Gd orbitals on the suppression of the ferroelectric property of the system. It was also found that $3d$-$4f$ magnetic coupling plays an important role in ferroelectric distortion. Further, we also found a large spin-phonon coupling of 3.02 cm^{-1} from the antisymmetric stretching mode [$A_g(7)$] considering only the symmetric Cr^{3+}-Cr^{3+} interaction, corroborating strong magnetoelectric coupling in this material, which provides a complementary tool for the enhancement of ferroelectric polarization.

ACKNOWLEDGMENTS

B.R. would like to thank Prof. P. V. Satyam for computational facilities, and S.D.M. would like to thank Insitute of Physics, Bhubaneswar, for kind hospitality. U.M. and D.T. would like to thank International Centre for Theoretical Physics (ICTP), Italy under the ICTP-Elettra users program for the financial support for experiments at Elettra, Italy.

[1] N. A. Hill, J. Phys. Chem. B **104**, 6694 (2000).
[2] R. E. Cohen, Nature (London) **358**, 136 (1992).
[3] G. Kwei, A. Lawson, S. Billinge, and S. Cheong, J. Phys. Chem. **97**, 2368 (1993).
[4] J. Wang, J. Neaton, H. Zheng, V. Nagarajan, S. Ogale, B. Liu, D. Viehland, V. Vaithyanathan, D. Schlom, U. Waghmare *et al.*, Science **299**, 1719 (2003).
[5] R. Seshadri and N. A. Hill, Chem. Mater. **13**, 2892 (2001).
[6] S.-W. Cheong and M. Mostovoy, Nat. Mater. **6**, 13 (2007).
[7] M. Kenzelmann, A. B. Harris, S. Jonas, C. Broholm, J. Schefer, S. B. Kim, C. L. Zhang, S.-W. Cheong, O. P. Vajk, and J. W. Lynn, Phys. Rev. Lett. **95**, 087206 (2005).
[8] T. Kimura, G. Lawes, T. Goto, Y. Tokura, and A. P. Ramirez, Phys. Rev. B **71**, 224425 (2005).
[9] H. Katsura, N. Nagaosa, and A. V. Balatsky, Phys. Rev. Lett. **95**, 057205 (2005).
[10] G. Giovannetti, S. Kumar, D. Khomskii, S. Picozzi, and J. van den Brink, Phys. Rev. Lett. **103**, 156401 (2009).
[11] B. B. Van Aken, T. T. Palstra, A. Filippetti, and N. A. Spaldin, Nat. Mater. **3**, 164 (2004).
[12] Y. Tokunaga, N. Furukawa, H. Sakai, Y. Taguchi, T.-h. Arima, and Y. Tokura, Nat. Mater. **8**, 558 (2009).
[13] Y. Tokunaga, S. Iguchi, T. Arima, and Y. Tokura, Phys. Rev. Lett. **101**, 097205 (2008).
[14] Y. J. Shan, H. Mori, K. Tezuka, H. Imoto, and M. Itoh, Ferroelectrics **284**, 107 (2003).
[15] H. Moriwake, A. Kuwabara, C. A. J. Fisher, H. Taniguchi, M. Itoh, and I. Tanaka, Phys. Rev. B **84**, 104114 (2011).
[16] N. A. Benedek and C. J. Fennie, Phys. Rev. Lett. **106**, 107204 (2011).
[17] N. A. Benedek, A. T. Mulder, and C. J. Fennie, J. Solid State Chem. **195**, 11 (2012).
[18] J. Young, A. Stroppa, S. Picozzi, and J. M. Rondinelli, J. Phys. Condens. Matter **27**, 283202 (2015).
[19] C. R. Serrao, A. K. Kundu, S. B. Krupanidhi, U. V. Waghmare, and C. N. R. Rao, Phys. Rev. B **72**, 220101 (2005).
[20] N. Ray and U. V. Waghmare, Phys. Rev. B **77**, 134112 (2008).
[21] J. R. Sahu, C. R. Serrao, N. Ray, U. V. Waghmare, and C. Rao, J. Mater. Chem. **17**, 42 (2007).
[22] U. V. Waghmare and K. M. Rabe, Phys. Rev. B **55**, 6161 (1997).
[23] K. Ramesha, A. Llobet, T. Proffen, C. Serrao, and C. Rao, J. Phys. Condens. Matter **19**, 102202 (2007).
[24] B. Rajeswaran, D. I. Khomskii, A. K. Zvezdin, C. N. R. Rao, and A. Sundaresan, Phys. Rev. B **86**, 214409 (2012).
[25] A. Apostolov, I. Apostolova, and J. Wesselinowa, Mod. Phys. Lett. B **29**, 1550251 (2015).
[26] V. S. Bhadram, B. Rajeswaran, A. Sundaresan, and C. Narayana, Europhys. Lett. **101**, 17008 (2013).
[27] A. Ghosh, K. Dey, M. Chakraborty, S. Majumdar, and S. Giri, Europhys. Lett. **107**, 47012 (2014).
[28] A. Ghosh, A. Pal, K. Dey, S. Majumdar, and S. Giri, J. Mater. Chem. C **3**, 4162 (2015).
[29] H. J. Zhao, L. Bellaiche, X. M. Chen, and J. Íñiguez, Nat. Commun. **8**, 14025 (2017).
[30] S. Mahana, U. Manju, and D. Topwal, J. Phys. D **50**, 035002 (2016).
[31] S. Mahana, U. Manju, and D. Topwal, AIP Conference Proceedings **1832**, 130046 (2017).
[32] J. P. Perdew, A. Ruzsinszky, G. I. Csonka, O. A. Vydrov, G. E. Scuseria, L. A. Constantin, X. Zhou, and K. Burke, Phys. Rev. Lett. **100**, 136406 (2008).
[33] G. Kresse and D. Joubert, Phys. Rev. B **59**, 1758 (1999).
[34] G. Kresse and J. Furthmüller, Phys. Rev. B **54**, 11169 (1996).
[35] H. J. Monkhorst and J. D. Pack, Phys. Rev. B **13**, 5188 (1976).
[36] A. Cooke, D. Martin, and M. Wells, J. Phys. C **7**, 3133 (1974).
[37] R. D. King-Smith and D. Vanderbilt, Phys. Rev. B **47**, 1651 (1993).
[38] A. Togo, F. Oba, and I. Tanaka, Phys. Rev. B **78**, 134106 (2008).
[39] J. Coey, M. Viret, and S. Von Molnar, Adv. Phys. **58**, 571 (2009).
[40] R. I. Hines, Ph.D. thesis, University of Bristol, 1997.
[41] A. Indra, K. Dey, A. Midya, P. Mandal, O. Gutowski, U. Rütt, S. Majumdar, and S. Giri, J. Phys. Condens. Matter **28**, 279601 (2016).
[42] S. F. Yuk, K. C. Pitike, S. M. Nakhmanson, M. Eisenbach, Y. W. Li, and V. R. Cooper, Sci. Rep. **7**, 43482 (2017).
[43] R. Wahl, D. Vogtenhuber, and G. Kresse, Phys. Rev. B **78**, 104116 (2008).
[44] H. T. Stokes and D. M. Hatch, J. Appl. Cryst. **38**, 237 (2005).

[45] H. T. Stokes, D. M. Hatch, and B. J. Campbell, isotropy software suite, http://iso.byu.edu.
[46] P. Ghosez, E. Cockayne, U. V. Waghmare, and K. M. Rabe, Phys. Rev. B **60**, 836 (1999).
[47] S. Bhattacharjee, E. Bousquet, and P. Ghosez, Phys. Rev. Lett. **102**, 117602 (2009).
[48] W. Zhong, R. King-Smith, and D. Vanderbilt, Phys. Rev. Lett. **72**, 3618 (1994).
[49] C. Ederer, T. Harris, and R. Kováčik, Phys. Rev. B **83**, 054110 (2011).
[50] W. Zhong and D. Vanderbilt, Phys. Rev. Lett. **74**, 2587 (1995).
[51] U. Aschauer and N. A. Spaldin, J. Phys. Condens. Matter **26**, 122203 (2014).
[52] M. Udagawa, K. Kohn, N. Koshizuka, T. Tsushima, and K. Tsushima, Solid State Commun. **16**, 779 (1975).
[53] M. C. Weber, J. Kreisel, P. A. Thomas, M. Newton, K. Sardar, and R. I. Walton, Phys. Rev. B **85**, 054303 (2012).
[54] V. S. Bhadram, D. Swain, R. Dhanya, M. Polentarutti, A. Sundaresan, and C. Narayana, Mater. Res. Express **1**, 026111 (2014).
[55] M. Balkanski, R. F. Wallis, and E. Haro, Phys. Rev. B **28**, 1928 (1983).
[56] Y. Sharma, S. Sahoo, W. Perez, S. Mukherjee, R. Gupta, A. Garg, R. Chatterjee, and R. S. Katiyar, J. Appl. Phys. **115**, 183907 (2014).
[57] E. Granado, A. García, J. A. Sanjurjo, C. Rettori, I. Torriani, F. Prado, R. Sánchez, A. Caneiro, and S. B. Oseroff, Phys. Rev. B **60**, 11879 (1999).
[58] M. Iliev, H. Guo, and A. Gupta, Appl. Phys. Lett. **90**, 151914 (2007).
[59] M. El Amrani, M. Zaghrioui, V. T. Phuoc, F. Gervais, and N. E. Massa, J. Magn. Magn. Mater. **361**, 1 (2014).
[60] T. Moriya, Phys. Rev. **120**, 91 (1960).
[61] A. McDannald, L. Kuna, M. Seehra, and M. Jain, Phys. Rev. B **91**, 224415 (2015).
[62] D. Lockwood and M. Cottam, J. Appl. Phys. **64**, 5876 (1988).
[63] R. Gupta, M. Kim, H. Barath, S. L. Cooper, and G. Cao, Phys. Rev. Lett. **96**, 067004 (2006).